

high-quality bulk samples (3–6). The normal-state resistivity at 290 K was $\sim 4.7 \mu\Omega \cdot \text{cm}$, indicating an intermetallic nature with a relatively high charge carrier density (2). This resistivity is smaller than those for polycrystalline MgB_2 wire (10) and for bulk samples synthesized under high pressure (3, 4). Most of our films fabricated under the same conditions showed a similar superconducting transition around 39 K.

Figure 2 shows the zero-field-cooled (ZFC) and the field-cooled (FC) dc magnetization (M) curves of a MgB_2 thin film in a 10-Oe field applied parallel to the c axis. The irreversibility temperature detected at 37.5 K coincides with the zero-resistance temperature obtained from measurements of resistivity. The ZFC curve shows a rather broad diamagnetic transition as compared to the resistivity data. To estimate the critical current density (J_c), we measured the M - H (H is magnetic field) loop for the same sample as a function of temperature, as shown in the inset of Fig. 2. At zero field, the J_c calculated with the Bean model was $\sim 6 \times 10^6 \text{ A/cm}^2$ at 5 K and $\sim 3 \times 10^5 \text{ A/cm}^2$ at 35 K, values that are 10 times higher than the values obtained for a MgB_2 wire (10) by means of transport measurements and slightly smaller than the values for Hg-based superconducting thin films (12). It should be noted that we used the sample size rather than the grain size in calculating J_c . In view of the strongly linked nature of the intergrains (9) and their excellent electrical and magnetic characteristics as compared to conventional superconductors, these films would be useful in electronic device applications, such as microwave devices and portable SQUID sensors, by using miniature cryocoolers with low power consumption.

Structural analysis was carried out by XRD (Fig. 3). The a - and c -axis lattice constants determined from the (101) and the (00 l) peaks are observed to be 0.310 and 0.352, respectively. The XRD patterns indicate that the films deposited on AO (Fig. 3A) are epitaxially aligned with the c axis, whereas the films on STO (Fig. 3B) are well aligned with the (101) direction normal to the substrate planes. These results suggest that we may be able to control the orientation of MgB_2 thin films simply by using different substrates if the optimum growth condition is explored. We also find that the AO substrates are chemically very stable during heat treatment at high temperatures in Mg vapor. With its high thermal conductivity and small dielectric constant, AO is a very promising substrate for use in superconducting device applications, such as microwave devices and portable sensors. For the STO substrates, however, a chemical reaction between the substrate and Mg was observed and appeared as minor impurity phases (Fig. 3A). Considering that STO has a cubic structure with a lattice constant of 0.389 nm and that R -plane

AO has $a_0 = 0.476 \text{ nm}$ and $b_0^* = (c_0^2 + 3a_0^2)^{1/2} = 1.538 \text{ nm}$, it is quite striking that MgB_2 thin films grow with preferred orientations on AO and STO substrates even though the lattice-matching relationship between the MgB_2 and the substrates is not well satisfied.

References and Notes

1. J. Nagamatsu *et al.*, *Nature* **410**, 63 (2001).
2. W. N. Kang *et al.*, preprint available at <http://xxx.lanl.gov/abs/cond-mat/0102313> (2001).
3. C. U. Jung *et al.*, preprint available at <http://xxx.lanl.gov/abs/cond-mat/0102215> (2001).
4. Y. Takano *et al.*, preprint available at <http://xxx.lanl.gov/abs/cond-mat/0102167> (2001).
5. D. K. Finnemore *et al.*, *Phys. Rev. Lett.* **86**, 2420 (2001).

6. H. Kotegawa *et al.*, preprint available at <http://xxx.lanl.gov/abs/cond-mat/0102334> (2001)
7. G. Karapetrov *et al.*, preprint available at <http://xxx.lanl.gov/abs/cond-mat/0102313> (2001).
8. S. L. Bud'ko *et al.*, *Phys. Rev. Lett.* **86**, 1877 (2001).
9. D. C. Labalestier *et al.*, *Nature* **410**, 186 (2001).
10. P. C. Canfield *et al.*, *Phys. Rev. Lett.* **86**, 2423 (2001).
11. A. Gupta, J. Z. Sun, C. C. Tsuei, *Science* **265**, 1075 (1994).
12. L. Krusin-Elbaum, C. C. Tsuei, A. Gupta, *Nature* **373**, 679 (1995).
13. W. N. Kang, R. L. Meng, C. W. Chu, *Appl. Phys. Lett.* **73**, 381 (1998).
14. Supported by the Creative Research Initiatives of the Korean Ministry of Science and Technology.

19 March 2001; accepted 2 April 2001
 Published online 12 April 2001;
 10.1126/science.1060822

Include this information when citing this paper.

Hydrated Salt Minerals on Ganymede's Surface: Evidence of an Ocean Below

Thomas B. McCord,* Gary B. Hansen, Charles A. Hibbitts

Reflectance spectra from Galileo's near-infrared mapping spectrometer (NIMS) suggests that the surface of Ganymede, the largest satellite of Jupiter, contains hydrated materials. These materials are interpreted to be similar to those found on Europa, that is, mostly frozen magnesium sulfate brines that are derived from a subsurface briny layer of fluid.

Ganymede is the third outward and the largest of Jupiter's four major satellites, named the Galilean satellites after their discoverer. These satellites range in size from slightly smaller than the Moon to larger than Mercury and are large enough to have undergone at least some internal thermal evolution and differentiation (1). There are three major sources of internal heat to support thermal evolution: (i) decay of radioactive isotopes; (ii) tidal dissipation, which is more effective on satellites closer to Jupiter; and (iii) differentiation, resulting from the first two processes. These processes operate on different time scales. Thus, the thermal evolution of these satellites should be complex and different for each satellite. Evidence of these processes should exist in the composition of the surface material. Because of their distance from the Sun, at the boundary where water ice is stable, these satellites probably formed from material rich in H_2O , such as found in primitive meteorites (2), and including water ice grains (3). Io, the closest Galilean satellite to Jupiter, is the most volcanically active body in the solar system and is thermally processed due to tidal heating such that most or all of the water has been lost. Early ground-based spectroscopic ob-

servations (4) provided evidence of water ice as a major constituent of the surfaces of the outer three satellites (Europa, Ganymede, and Callisto). Water ice on the surface is probably the result of thermal processing of water and water-bearing material originally forming the satellites, leading to differentiation and migration of water to the surface layers and production of hydrated minerals as water circulates through and leaches ions from the satellite materials (5–8). Recently, the NIMS provided evidence of materials other than water ice on the icy satellites (9). These include non-water ice but H_2O -bearing material on Europa. The material is preferentially located in the lineaments and chaos terrain (recently disrupted areas) and was interpreted to be mostly hydrated salt minerals, mostly MgSO_4 and possibly Na_2SO_4 , derived from a briny ocean below the ice crust (10–12). H_2SO_4 hydrate also has been suggested as a constituent due to radiolysis of sulfur and ice at the surface (13). Some H_2SO_4 hydrate could be present as a result of radiation processing of the minority Na_2SO_4 hydrate mixed with the majority MgSO_4 hydrate (12, 14). Hydrated salt minerals on and in the more processed icy satellites are predicted by models of the thermal evolution of the Galilean satellites and studies of carbonaceous chondrite meteorites (5–8).

Evidence of hydrated minerals on the surface of the Galilean satellites comes from infrared reflectance spectra. Water molecules

Hawaii Institute of Geophysics and Planetology, University of Hawaii, Honolulu, Hawaii.

*To whom correspondence should be addressed. E-mail: tom@higp.hawaii.edu

show strong absorptions in the 1- to 3- μm spectral region, in particular near 1.4, 1.9, and 2.8 μm . The characteristics of these absorptions change from those for water ice as H_2O becomes bound in a hydrated mineral, and they vary depending on the particular mineral, the bonding configurations, the number of waters of hydration involved, and temperature (11, 12). For Europa, the evidence for hydrated minerals such as $\text{MgSO}_4 \cdot x\text{H}_2\text{O}$ is the highly distorted water absorptions found for some areas compared with the more symmetrical absorptions for water ice, especially near 1.4 and 1.9 μm .

For Ganymede, ground-based spectra of the entire satellite disk suggested the presence of ice as well as non-ice material (4, 15, 16) on the surface, results that were confirmed by the NIMS observations (17, 18). We attempted to identify the non-ice materials on Ganymede by searching the NIMS spatially resolved data for non-ice mineral spectral signatures. This search is complicated by the near omnipresence of water ice, with water ice and non-ice signatures mixed in every NIMS pixel. The water ice spectral signature is particularly concentrated at the poles and away from the trailing side, and both amorphous and crystalline forms are evi-

dent (18). The trailing side shows evidence of mostly large-grained ($>300 \mu\text{m}$) ice. Elsewhere, fine-grained ($<100 \mu\text{m}$) ice tends to dominate the spectral signature in the spectral range studied here. This is consistent with sputtering that preferentially removes ice from the trailing side and redeposits the water molecules as a frost elsewhere, especially at colder sites such as the poles and higher albedo areas.

We proceeded by selecting NIMS reflectance spectra for areas on Ganymede that showed the most broadened and distorted, i.e., non-ice-like, water absorptions. These exist in many areas that are darker in the visible spectral range. We also used radiative transfer models to develop water ice spectra for a variety of grain sizes (11). Examples of these were subtracted from the NIMS reflectance spectra in an attempt to remove the effects of water ice and obtain purer spectra of the non-ice material. This approach assumes the surface is made up of discrete patches of non-ice and ice material,

i.e., little or no intimate mixing that would lead to multiscattering. This model worked successfully for some areas, suggesting that the frost deposits, at least at these locations, occur in patches on the surface. The patches may be due to an uneven surface temperature distribution (brighter areas tend to be colder), resulting in uneven cold-trapping of H_2O molecules, and/or due to down-slope movement of weathered-out dark material, forming ponds in low elevations (19) seen in some images from the Galileo solid-state imager (SSI) investigation (20). Further, in the regions where the most hydrate-like spectra occur, the water ice present seems to be mostly large grained, about 2 mm in radius. This makes removal of the water ice spectral signature easier because large-grained ice tends to be mostly black except at the shortest wavelengths in the spectral region studied by NIMS.

We selected two examples of NIMS reflectance spectra for Ganymede that show asymmetric water of hydration absorption bands, especially near 1.5 and 2.0 μm (a at 27°S, 259°W and b at 3°N, 274°W) (Fig. 1A). These two locations are in darker regions on the trailing side of Ganymede and are geologically mapped as dark or ancient cratered terrain (21, 22). When the effect of large-grained ($\sim 2 \text{ mm}$) water ice contaminating the non-ice spectral signature is removed, spectra more representative of the non-ice material result (a' and b' in Fig. 1B). The water ice spectrum used (Fig. 1B) affects mostly the shorter wavelength region because large-grained ice absorbs light strongly toward longer wavelengths.

The two Ganymede hydrated mineral spectra a' and b' are compared with Europa's spectrum of hydrated minerals (Fig. 2A). A water ice spectrum for 50- μm ice grains is also shown to illustrate the difference in the water band absorption shapes and positions. Note the similarity between the Ganymede and Europa hydrated mineral spectra, especially for the 1.5- and 2.0- μm water absorptions. This similarity is better illustrated by scaling and plotting Europa's absorption bands over Ganymede's spectra (Fig. 2B). The water of hydration absorptions are identical in both shape and wavelength position within the precision of the measurements. This is evidence of similar hydrated materials on both satellites.

The main difference between the hydrated mineral spectra of the two satellites is that Europa's spectrum slopes downward toward longer wavelengths more strongly than Ganymede's. This could be partly explained by a difference in the grain sizes of the hydrated mineral between Europa and Ganymede. Larger grain sizes tend to have steeper slopes, as for Europa (23). Further, in our laboratory simulations of the rapid deposition of brines onto the Europa surface (12), we noted that in most cases the more hydrated the mineral, the steeper the slope of the spectrum. For MgSO_4 brines,

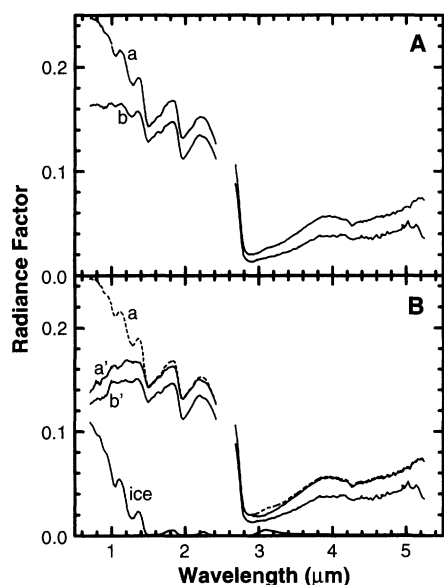


Fig. 1. (A) Two examples of reflectance spectra for regions (about 80 km by 80 km) of Ganymede from the Galileo NIMS investigation. These are for the E6 global observation. The pixels are located at $27 \pm 2^\circ\text{S}$, 259°W (spectrum a) and 3°N , 274°W (spectrum b). The instrument pixel size is about 160 km per side for this data set. The pixels were nyquist sampled and then were projected and re-sampled to 80-km pixels for analysis. Data are missing between 2.4 and 2.7 μm because of a failed detector in NIMS. (B) The same spectra from (A) after an attempt to remove the effects of water ice on the Ganymede spectra, labeled a' and b'. The water ice spectrum subtracted from spectrum a is shown at the bottom of (B). Spectrum a from (A) is repeated in (B).

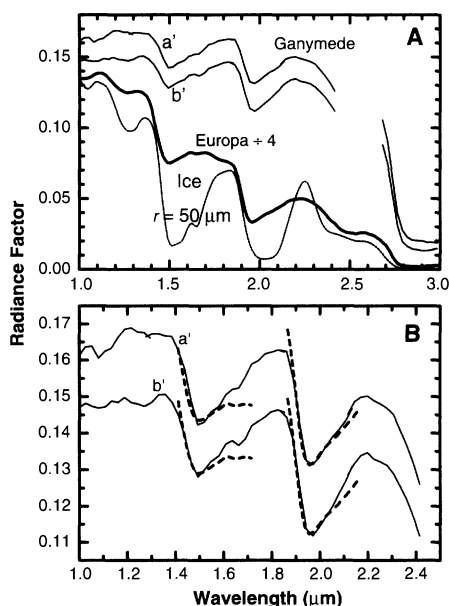


Fig. 2. (A) Shown here are the ice-removed Ganymede spectra from Fig. 1B compared with the Europa hydrate mineral end-member spectrum (72), which has been scaled by multiplying by 0.25. Also shown is a representative water ice spectrum for grains of radii of 50 μm to illustrate the difference in the H_2O band shapes and positions between ice and hydrated minerals (11). (B) The two ice-removed Ganymede hydrate spectra from Fig. 1B are shown with the spectrum for the two strong H_2O absorption bands for Europa's hydrate mineral end-member spectrum (A). The Europa spectrum for the two bands is scaled and offset to show the closest overlay with the Ganymede spectra as follows: For spectrum a', multiply the short band spectrum by 0.15 and add an offset of 0.0985 and then multiply the long band spectrum by 0.25 and add an offset of 0.098. For spectrum b', multiply the short band spectrum by 0.15 and add an offset of 0.084 and then multiply the long band spectrum by 0.25 and add an offset of 0.079.

A Silent Slip Event on the Deeper Cascadia Subduction Interface

Herb Dragert,* Kelin Wang, Thomas S. James

Continuous Global Positioning System sites in southwestern British Columbia, Canada, and northwestern Washington state, USA, have been moving landward as a result of the locked state of the Cascadia subduction fault offshore. In the summer of 1999, a cluster of seven sites briefly reversed their direction of motion. No seismicity was associated with this event. The sudden displacements are best explained by ~2 centimeters of aseismic slip over a 50-kilometer-by-300-kilometer area on the subduction interface downdip from the seismogenic zone, a rupture equivalent to an earthquake of moment magnitude 6.7. This provides evidence that slip of the hotter, plastic part of the subduction interface, and hence stress loading of the megathrust earthquake zone, can occur in discrete pulses.

the shape and position of the two water of hydration bands (Fig. 2) did not change much for seven or more waters of hydration, but the slope of the spectrum increased with degree of hydration beyond about seven waters (12). Thus, the hydrated minerals on Europa could be more hydrated and/or of a larger grain size than on Ganymede. Lastly, a third material other than water ice and hydrated minerals could be present, reducing the slope of the spectrum for Ganymede.

These results suggest that brines or deposits formed from brines reached the surface on Ganymede at some time. This is consistent with the interpretation of results from the Galileo magnetometer investigation, suggesting a conducting fluid layer just beneath the surface of Ganymede (24). It is also consistent with the identification of regions on Ganymede that apparently have experienced severe surface disruptions, similar to that seen on Europa (25). Thus, Ganymede, like Europa, may have a large fluid region or regions beneath its icy crust. We suggest that this liquid is a brine rich in $MgSO_4$ and that some of the brine material reached the surface of Ganymede over the history of its evolution.

References and Notes

- J. D. Anderson et al., *Science* **276**, 1236 (1997).
- E. R. Du Frenesne, E. Anders, *Geochim. Cosmochim. Acta* **26**, 1058 (1962).
- F. P. Fanale, J. R. Salvail, *Icarus* **82**, 97 (1989).
- W. M. Calvin et al., *J. Geophys. Res.* **100**, 19041 (1995).
- F. P. Fanale, T. V. Johnson, D. L. Matson, in *Planetary Satellites* (Univ. of Arizona Press, Tucson, AZ, 1977), pp. 379–405.
- J. S. Kargel, *Icarus* **94**, 368 (1991).
- F. P. Fanale et al., *Lunar Planet. Sci.* **XXIX**, 1248 (abstr.) (1998).
- M. Y. Zolotov and E. L. Shock, *J. Geophys. Res.*, in press.
- T. B. McCord, *Eos* **81**, 209 (2000).
- T. B. McCord et al., *Science* **280**, 1242 (1998).
- T. B. McCord et al., *J. Geophys. Res.* **104**, 11824 (1999).
- T. B. McCord et al., *J. Geophys. Res.*, in press.
- R. W. Carlson, R. E. Johnson, M. S. Anderson, *Science* **286**, 97 (1999).
- T. B. McCord et al., *J. Geophys. Res.* **106**, 3311 (2001).
- C. B. Pilcher et al., *Science* **178**, 1087 (1972).
- R. N. Clark, T. B. McCord, *Icarus* **41**, 323, (1980).
- T. B. McCord et al., *J. Geophys. Res.* **103**, 8603 (1998).
- G. B. Hansen, T. B. McCord, *Eos* **81**, F792 (2000).
- J. R. Spencer, *Icarus* **69**, 297 (1987).
- J. M. Moore et al., *Icarus* **140**, 294 (1999).
- D. E. Wilhelms, U.S. Geol. Surv. Misc. Investig. Map I-2442 (1997); S. K. Croft, R. Casacchia, R. G. Strom, U.S. Geol. Surv. Misc. Investig. Map I-2328 (1994). From Galileo images, G. C. Collins made a GIS map of Ganymede that identifies a generic "dark terrain" within which our spots lie. A low-resolution map is presented in G. C. Collins, J. W. Head, R. T. Pappalardo, Galileo SSI Team, *Lunar Planet. Sci.* **XXXI**, 1034 (abstr.) (2000).
- G. Shoemaker et al., in *Satellites of Jupiter* (Univ. of Arizona Press, Tucson, AZ, 1982), pp. 435–520.
- L. Van Keulen et al., *Lunar Planet. Sci.* **XXXI**, 1539 (abstr.) (2000).
- M. G. Kivelson, *Eos* **81**, F789 (2000).
- R. T. Pappalardo et al., *Eos* **81**, F791 (2000).
- We thank F. Fanale and R. Pappalardo for helpful comments. Supported by NASA grants NAG5-10514, NAG5-8983, and JPL-960443. This is University of Hawaii publication no. 1145 (HIGP) and 5470 (SOEST).

Great thrust earthquakes [moment magnitude (M_w) > 8] repeatedly rupture the shallow (<25 km) portion of the Cascadia subduction interface (1, 2) where the oceanic Juan de Fuca plate descends beneath the North America plate (Fig. 1). Geodetic measurements over the past decade at sites on the Cascadia margin have confirmed that this seismogenic zone of the subduction fault is currently locked (3–9). Continuous motion of the converging plates produces tectonic loading of the locked segment, eventually leading to earthquake rupture. Downdip from the seismogenic zone, temperature-controlled rheology and friction allow smoother slip without producing earthquakes (10). If there is instability in the deep segment caused by time-varying rheology or friction, the aseismic slip may be episodic and could at times trigger an earthquake in the updip seismogenic zone (11–13). The mode of the aseismic slip below the seismogenic zone of subduction faults between great earthquakes has not been observationally constrained, although theory suggests that plastic instabilities in the pressure-temperature environment of the upper mantle and lower crust may give rise to transient enhancement of slip rates (14). Data from a contiguous set of seven continuous Global Positioning System (GPS) sites have now provided evidence for the occurrence of sudden aseismic slip over a large area of the deeper Cascadia subduction interface.

Analyses of GPS data are routinely carried out for the 14 continuous GPS sites identified in Fig. 1. These sites were established specifically for the study of crustal motions (15). Changes in the latitude, longitude, and height of sites

relative to the GPS site at Penticton (DRAO) are estimated from daily data (16).

To reduce further day-to-day scatter that is common to all sites of the network, daily residuals in individual components are computed for each site by removing linear trends, annual signals, and steps due to antenna set-up changes and the slip event identified in this study, all estimated simultaneously by least-mean-squares regression. These daily residuals are averaged for all network sites, and these averages are subtracted from the raw time series (Fig. 2). The application of this regional filter reduces the means of the daily (rms) scatter in the north, east, and up components from 1.3, 1.4, and 4.7 mm to 0.8, 0.8, and 3.1 mm, respectively.

Processing data with this precision has resulted in the identification of an unexpected episode of displacements at seven contiguous sites (Table 1 and Fig. 3). Total horizontal displacements, estimated from regression, ranged from 2 to 4 mm. Estimates of the time span for the displacements at individual sites ranged from 6 to 15 days (Table 1 and Fig. 2). The longer term northeastward motion of these sites, largest at outer coastal sites, is consistent with convergence between the Juan de Fuca and North America plates with no slip at the locked part of the subduction boundary that underlies the offshore continental slope. The newly detected transient motion is in the opposite direction of this northeastward motion (Fig. 1), and displacements are largest at ALBH and PGC5, sites that are located more than 100 km landward of the locked zone. The displacements attenuate rapidly to the east and south and less rapidly to the west and northwest. The time of their occurrence varies systematically, being earliest in the southeast and about 35 days later in the northwest region of detection, indicating a signal propagation parallel to the strike of the subducting slab at an equivalent

Geological Survey of Canada, Pacific Geoscience Centre, 9860 West Saanich Road, Sidney, British Columbia, Canada V8L 4B2.

*To whom correspondence should be addressed. E-mail: dragert@pgc.nrcan.gc.ca

15 February 2001; accepted 19 April 2001